Geostationary Environment Monitoring Spectrometer (GEMS): Long-Term Radiometric Accuracy and Spectral Stability From 4.5 Years of On-Orbit Solar Irradiance Observations

Juseon Bak, Kai Yang, Arno Keppens, Mijeong Kim, Xiong Liu, Jae-Hwan Kim, Jhoon Kim, *Member, IEEE*, Myoung-Hwan Ahn, *Member, IEEE*, Heesung Chong, Sungjae Hong, Kyunghwa Lee, Mina Kang, Won-Jin Lee, *Member, IEEE*, and Hyunkee Hong

***Abstract*—The Geostationary Environment Monitoring Spectrometer (GEMS), the first ultraviolet–visible (UV) hyperspectral imager in geostationary orbit, has been operating since its launch in February 2020. This article evaluates and discusses the on-orbit performance of GEMS using 4.5 years of irradiance measurements (300–500 nm), with a particular emphasis on the long-term changes in its radiometric accuracy and spectral stability. As part of this assessment, we examine various super-Gaussian forms used for deriving on-orbit slit functions and conclude that applying symmetry constraints to both shape and width parameters enhances fitting stability and accuracy. During the initial phase of operation, the full-width at half-maximum (FWHM) of the derived slit functions ranged from 0.56 to 0.58 nm across spatial and spectral dimensions. The wavelength shift remains spatially uniform and varies smoothly within ±0.05 nm, showing a consistent, repeating pattern in 300–400 and 400–500 nm. However, over time, instrument degradation has led to pronounced spectral and spatial variations, particularly at shorter wavelengths. Slit widths (FWHM) at the center pixels fluctuate between 0.54 and 0.60 nm, and a "frown-shaped" spatial pattern emerges in the wavelength shift. Radiometric offsets exhibit a steady increase—approximately 5% per year at shorter wavelengths below 330 nm and 0.2% above 460 nm. By 2024, irradiance values are up to 35% lower near 325 nm and about 10% lower above 460 nm compared to the solar reference. To isolate fine-scale uncertainties, we further evaluate the fitting residuals between the measured irradiance and the radiometrically adjusted solar reference. As the degradation progressed, residuals in 310–330 nm increased sharply from 0.4% in 2020 to 4% in 2024, while fitting uncertainties nearly doubled in 330–360 nm. This degradation feature indicates the emergence of instrumental artifacts in spectral structures that are unrelated to physical solar absorption features. Such artifacts are most pronounced at the central pixels and have gradually extended toward the southern pixels and adjacent spectral regions throughout the mission. Beyond 400 nm, radiometric offsets occur on a broadband scale, with no noticeable degradation in the fine spectral structures.**

***Index Terms*—Geostationary Environment Monitoring Spectrometer (GEMS), on-orbit slit function, radiometric degradation, wavelength shift.**

Received 31 March 2025; revised 24 June 2025, 11 August 2025, and 11 September 2025; accepted 19 October 2025. Date of publication 3 November 2025; date of current version 16 December 2025. This work was supported in part by the Basic Science Research Program of the National Research Foundation of Korea (NRF) funded by the Ministry of Education under Grant RS-2020-NR049592 and Grant RS-2021-NR058144 and in part by the National Institute of Environment Research (NIER) under Grant NIER-2025-04-02-063. *(Corresponding author: Juseon Bak.)*

Juseon Bak is with the Institute of Environmental Studies, Pusan National University, Busan 46241, South Korea (e-mail: juseonbak@pusan.ac.kr).

Kai Yang is with the Department of Atmospheric and Oceanic Science, University of Maryland, College Park, MD 20742 USA (e-mail: kaiyang@umd.edu).

Arno Keppens is with the Royal Belgian Institute for Space Aeronomy (BIRA-IASB), 1180 Brussels, Belgium (e-mail: arno.keppens@aeronomie.be).

Mijeong Kim, Kyunghwa Lee, Won-Jin Lee, and Hyunkee Hong are with the Environmental Satellite Center, Atmospheric Environmental Research Department, National Institute of Environmental Research (NIER), Incheon 22689, South Korea (e-mail: mjkim48@korea.kr; nierkhlee@korea.kr; wjleeleo@korea.kr; wanju77@korea.kr).

Xiong Liu and Heesung Chong are with the Atomic Molecular Physics Division, Center for Astrophysics|Harvard & Smithsonian, Cambridge, MA 02138 USA (e-mail: xliu@cfa.harvard.edu; heesung.chong@cfa.harvard.edu).

Jae-Hwan Kim and Sungjae Hong are with the Department of Atmospheric Sciences, Pusan National University, Busan 46241, South Korea (e-mail: jaekim@pusan.ac.kr; sungjae@pusan.ac.kr).

Jhoon Kim is with the Department of Atmospheric Sciences, Yonsei University, Seoul 03722, South Korea (e-mail: jkim2@yonsei.ac.kr).

Myoung-Hwan Ahn is with the Department of Climate and Energy Systems Engineering, Ewha Womans University, Seoul 03760, South Korea (e-mail: terryahn65@ewha.ac.kr).

Mina Kang is with the Research Foundation of the City University of New York (RFCUNY) and the National Oceanic and Atmospheric Administration Cooperative Science Center for Earth System Sciences and Remote Sensing Technologies (NOAA-CESSRST), New York, NY 10031 USA (e-mail: mkang@ccny.cuny.edu).

Digital Object Identifier 10.1109/TGRS.2025.3627802

I. Introduction

SATELLITE remote sensing of atmospheric composition and surface properties relies on precise measurements of direct solar irradiance and backscattered Earth radiance. Solar irradiance is well characterized and serves as a fundamental reference for evaluating radiometric calibration accuracy and detecting instrumental artifacts [1], [2], [3]. In trace gas retrievals, normalizing radiance by solar irradiance enhances atmospheric absorption features by removing solar Fraunhofer lines and mitigating instrumental effects that are common to both radiance and irradiance measurements [4]. Furthermore, solar irradiance observations play a crucial role in monitoring solar activity and its influence on Earth's atmosphere [5], [6]. The stability and reliability of these measurements directly affect the accuracy of the derived atmospheric products,

thereby affecting their application in scientific research and environmental monitoring [7].

In space-based air quality monitoring, the Geostationary Environment Monitoring Spectrometer (GEMS) stands out as the world's first ultraviolet–visible (UV) hyperspectral imager operating in a geostationary orbit. Launched in February 2020 onboard the Geostationary Korea Multi-Purpose Satellite-2B (GK2B) [8], GEMS provides hourly daylight measurements of backscattered Earth radiance over East Asia and daily nighttime measurements of direct solar irradiance, enabling continuous monitoring of ozone (O_3), aerosols, and their precursors, including nitrogen dioxide (NO_2), sulfur dioxide (SO_2), formaldehyde (HCHO), and glyoxal (CHOCHO) [9], [10], [11], [12]. It precedes other geostationary air quality missions such as TEMPO (North America, launched in 2023) [13] and Sentinel-4 (Europe, launched in 2025) [14], positioning GEMS as a pioneering mission in this observational domain.

Kang et al. [15] determined the prelaunch GEMS Instrument Spectral Response Functions (ISRFs) using monochromatic laser measurements during an extensive on-ground calibration campaign. They further recommended the use of an asymmetric super-Gaussian model to derive GEMS slit functions from solar irradiance measurements, citing the consistency between prelaunch measurements and on-orbit derivations, as well as minimal variations in the first year of operation. In [16], the focus shifted to the radiometric uncertainty in irradiance values, revealing spatial and seasonal discrepancies of approximately 15% compared with the high-resolution solar reference spectrum from [1]. This level of deviation substantially exceeds the radiometric calibration accuracy requirement of better than 4% [8]. Such discrepancies are primarily attributed to irradiance goniometry effects associated with the bidirectional transmittance distribution function (BTDF), which depends on both the azimuth and elevation angles of incoming light [18], [19]. For GEMS, BTDF measurements performed during the on-ground calibration campaign were insufficient to characterize its azimuth-dependent features in orbit. These uncharacterized goniometric dependencies directly contribute to the seasonal variability observed in GEMS total ozone uncertainties, as reported in [9], through comparisons with Pandora observations. In aerosol optical depth (AOD) retrievals [10], a solar reference spectrum is used instead of measured irradiance. To address the BTDF issue in irradiance measurements, Kang et al. [16] developed an empirical correction that uses the correlation between the azimuth angle and irradiance measurements. However, this correction has not yet been incorporated into the GEMS data processing pipeline due to remaining issues with residual BTDF effects, sensor degradation, and incomplete detection of hot or defective pixels.

In this study, we assess both spectral and radiometric calibration uncertainties in GEMS irradiances, with a particular emphasis on their long-term changes. The GEMS irradiances were characterized across instrument dimensions (spatial and spectral) over the 4.5 years since the start of nominal operations in November 2020. The derivation of on-orbit slit functions was revisited to evaluate the necessity of asymmetric factors in the super-Gaussian model, assessing their impact on the stability and accuracy of the spectral fitting between the GEMS radiances and the high-resolution solar reference spectrum. To assess spectral stability, we evaluate three important metrics for each retrieval fitting window of GEMS operational trace gas products: consistency of spectral response, accuracy of wavelength, and residuals from spectral fitting. Furthermore, GEMS measurements were evaluated against the high-resolution solar reference spectrum from [20], both with and without the radiometric offset, to characterize the underlying calibration biases.

II. Instrument, Dataset, and Methodology

A. GEMS Operations

The GEMS instrument operates in a geostationary orbit at an altitude of 35 786 km above the equator at 128.25°E, measuring both solar irradiance and Earth backscattered radiance using a single 2-D charge-coupled device (CCD) detector [8], [21]. The column dimension of the detector is utilized for 1033 wavelength bins spanning 300–500 nm, while the row dimension aligns with the north–south direction, simultaneously capturing 2048 spatial pixels. For Earth measurements, GEMS scans a 5000-km east–west swath through approximately 700 mirror steps. The same optical elements are used for both the Earth radiance and solar irradiance measurements, except for a set of solar diffusers (working and reference) with different operating intervals (daily and semiannually) to attenuate sunlight intensity and prevent detector saturation. Solar irradiance is measured once per day at night, while Earth radiance is observed eight times per day on average, typically between 09:00 and 16:00 Korea Standard Time (KST), and the number and scanning schedule of Earth observations vary depending on the month. The on-orbit test (IOT) was carried out from March to October 2020, and operational products have been officially released through the NIER website (https://nesc.nier.go.kr/). The Level-1C products have remained at version 2 for irradiance and 1.2.4 for radiance throughout the entire available period. The data processing chain consists of two main components [17]: the L0–L1B processor, which applies prelaunch instrument characterization and calibration, and the L1B–L1C processor, which addresses on-orbit corrections. The L0–L1B processor calibrates measurements for nonlinearity, smear, pixel response nonuniformity (PRNU), dark current, stray light, and BTDF effects related to the incident solar elevation angle (diffuser transmittance). GEMS was originally scheduled to observe the Sun at a 30° elevation angle, but this was changed to 30.5° to coordinate with the operations of the Geostationary Ocean Color Imager-II (GOCI-II) aboard the same GK-2B satellite. The prelaunch BTDF characterization was sufficient to account for this elevation angle change. However, the lack of incident azimuth–angle characterization has led to significant inaccuracies in the irradiance measurements. The L1B–L1C processor also corrects wavelength shifts in radiance and irradiance, respectively, relative to a reference spectrum in two spectral regions: 300–400 and 400–500 nm. For solar measurements, a high-resolution solar reference spectrum from [22] is used, while Earthshine measurements are spectrally aligned using the ozone absorption cross section from [23]. The on-orbit slit function, derived assuming a standard Gaussian, is applied in both wavelength calibrations to represent the GEMS spectral resolution.

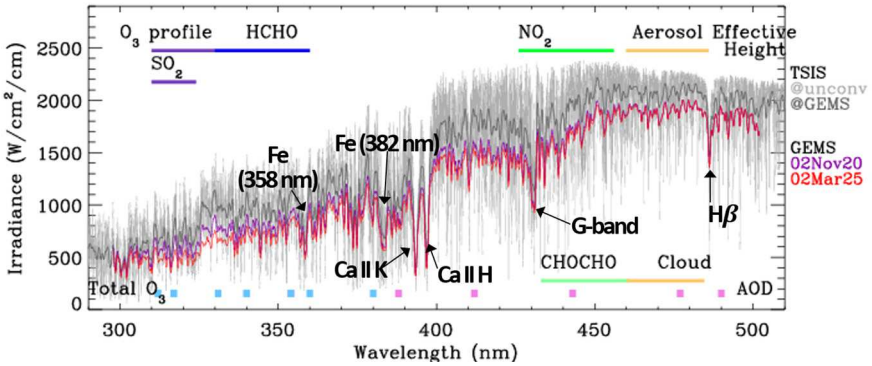

Fig. 1. GEMS solar irradiance at the center spatial pixel, measured on November 2, 2020 (purple), and March 2, 2025 (red), normalized to an Earth–Sun distance of 1 AU. The high-resolution solar reference spectrum [20] is shown in light gray, and its convolution with the GEMS prelaunch ISRFs is shown in dark gray. Prominent Fraunhofer lines are indicated with arrows. Colored horizontal bars denote the spectral ranges used in the GEMS level 2 algorithms.

In this work, GEMS solar irradiances, originally provided in $W/cm^2/cm$ at the true Earth–Sun distance, are adjusted to Sun–Earth normalized irradiances at 1 astronomical unit (AU) to remove seasonal variations in solar distance. Fig. 1 illustrates the noticeable changes in irradiance values over 4.5 years, as well as the discrepancies with the reference spectrum.

B. Reference Spectrum Simulation

To evaluate the radiometric accuracy of the measured spectrum, the high-resolution reference spectrum (I_h) is first spectrally resampled and adjusted to match the instrument's spectral resolution and wavelength alignment. The resulting instrument-sampled reference spectrum (I_{ref}) is given by

$$I_{\text{ref}}(\lambda) = I_h(\lambda+\Delta\lambda) \otimes S(x) \tag{1}$$

where $\Delta\lambda$ is the wavelength calibration parameter that corrects for spectral shifts between the measured and referenced spectra, thereby ensuring proper alignment of Fraunhofer lines. The ISRF or slit function, denoted as $S(x)$, represents the spectral resolution of the instrument, with x indicating the spectral displacement relative to the central wavelength.

To address radiometric offsets and other systematic discrepancies, scaling and baseline adjustments are applied as

$$I_{\text{ref}}(\lambda) = A \cdot I_h(\lambda + \Delta\lambda) \otimes S(x) \times P_s^m(\lambda) + P_b^m \tag{2}$$

where A is a scalar normalization factor, defined as the ratio of the average measured to the average simulated spectrum. The terms $P_s^m(\lambda)$ and $P_b^m(\lambda)$ are mth-order polynomials that represent multiplicative scaling and additive baseline corrections, respectively. Equation (1) is primarily used to assess the broad radiometric biases, while (2) allows for the evaluation of fine-scale uncertainties.

To determine fitting parameters, we employ the elastic least squares for nonlinear constraints (ELSUNC) algorithm [24], which iteratively minimizes the weighted square difference between the measured and simulated solar (reference) spectrum to find the optimal solution. In addition, analytical ISRF variables (e.g., slit width and shape factor) are included in the fitting process for retrieving on-orbit slit functions. Section II-C describes the high-resolution solar reference dataset, while Section II-D covers GEMS prelaunch ISRF measurements and the formulas used to define on-orbit ISRFs.

C. High-Resolution Solar Reference Spectrum

In this study, the Total and Spectral Solar Irradiance Sensor-1 (TSIS-1) hybrid solar reference spectrum (HSRS) [20], hereafter referred to as the TSIS-1 spectrum, served as a reference for assessing the GEMS irradiances. It spans 202–2730 nm at a 0.01–0.001-nm spectral resolution. The radiometric accuracy of the TSIS-1 spectrum is 0.3% in the short UV range of interest, a significant improvement over the 4%–5% uncertainty in existing solar reference datasets [1], [22]. The KNMI solar reference spectrum of [1] was used for GEMS validation by [15] and [16]. Bak et al. [25] confirmed a 1% radiometric discrepancy and a 0.001-nm spectral misalignment between the TSIS-1 and KNMI spectra in 310–330 nm.

D. Instrument Spectral Response Functions

Prior to launch, the GEMS ISRFs were characterized using monochromatic light sources for seven specific nominal wavelengths (301.8, 330, 365, 390, 435, 470, and 498.2 nm) across the full spatial extent of the detector. The instrument's spectral line shape features thinner wings and a more pronounced peak compared to a normal distribution. To generalize this characterization across the full spectral range, Kang et al. [15] constructed a lookup table by interpolating the measured ISRFs over all 1033 wavelength grids and also recommended the use of an asymmetric super-Gaussian function [26] to represent the on-orbit slit functions for GEMS

$$S(x) = S_0 \times \begin{cases} \exp\left(-\left|\dfrac{x}{w-a_w}\right|^{k-a_k}\right), & x \le 0 \\ \exp\left(-\left|\dfrac{x}{w+a_w}\right|^{k+a_k}\right), & x > 0 \end{cases} \tag{3}$$

where the normalization factor S_0 is empirically determined such that the normalization condition is satisfied

$$\int_{-\infty}^{\infty} S(x)\, x = 1. \tag{4}$$

This formulation simplifies to a symmetric super-Gaussian function when $a_w = a_k = 0$ and further reduces to a standard Gaussian function when the shape factor $k = 2$

$$S(x) = S_0 \times \exp\left(-\left|\frac{x}{w}\right|^k\right) \tag{5}$$

$$G(x) = S_0 \times \exp\left(-\frac{1}{2}\left(\frac{x}{\sigma}\right)^2\right) \quad (6)$$

where σ and w represent the half-width of a distribution at half-maximum and at 1/eth maximum, respectively. The full-width at half-maximum (FWHM) of the super-Gaussian is given by:

$$\text{FWHM} = 2\sqrt[k]{\ln 2}\, w. \quad (7)$$

III. Result

A. Temporal-, Spatial-, and Spectral-Dependent Features in Irradiance Measurements

The extraterrestrial solar irradiance exhibits natural fluctuations, primarily due to the Sun's roughly 27-day rotation and its 11-year sunspot cycle [27]. This variability, which is more pronounced in Fraunhofer lines than in the continuum, reaches about 1% in the UV band and decreases to approximately 0.1% in the visible band [28], [29]. Meanwhile, systematic biases and long-term changes observed in irradiance measurements are largely attributed to absolute calibration uncertainties and optical degradation. In GEMS data processing, the absence of a calibration element that accounts for the azimuth angle dependence of the solar diffuser's BTDF leads to angular dependence in the solar irradiances [16]. This overwhelming impact of BTDF makes it difficult to isolate and evaluate other underlying sources of uncertainty. Thus, mitigating the BTDF effect is critical for accurately assessing the long-term stability discussed in this article. To support this, we characterize the spatiotemporal patterns of irradiance measurements as the basis for evaluation.

Specifically, monthly means and standard deviations of irradiance measurements at 400.2 nm (the center of the wavelength grids) are used to identify systematic biases and assess short-term stability, respectively. As shown in Fig. 2(a), the monthly mean irradiance exhibits a clear seasonal cycle with a unimodal pattern. The amplitude of this seasonal variation differs across spatial pixels, being more pronounced at the edge (e.g., xpos: 50 and 2000) and weaker near the center (e.g., xpos: 1024). Notably, the spatial dependence is most evident during the solstices, being larger by a factor of two during the winter solstice compared to the summer solstice. This pattern is closely related to the incident azimuth angle, as shown in Fig. 2(c). During the solstices, the azimuth angle reaches its extremes, enhancing the BTDF-induced angular dependence across the field of view, whereas, during the equinoxes, the Sun rises directly east and sets directly west regardless of latitude, resulting in nearly uniform azimuth angles. Meanwhile, the monthly standard deviations of daily irradiance measurements reach their minimum (~0.05%) at the solstices and maximum (> 0.5%) at the equinoxes [see Fig. 2(b)]. This seasonal dependence of short-term variability is primarily driven by BTDF-induced fluctuations associated with daily changes in the incident azimuth angle.

We further characterize irradiance variations across all wavelengths and spatial pixels of the CCD frame. The monthly mean data for June are compared between consecutive years when short-term variability is minimal [see Fig. 3(a)–(c)]. In the long-wavelength grids above 450 nm, the radiometric change remains below 0.2% per year across spatial pixels, whereas, in the ozone profile fitting window (310–330 nm), it

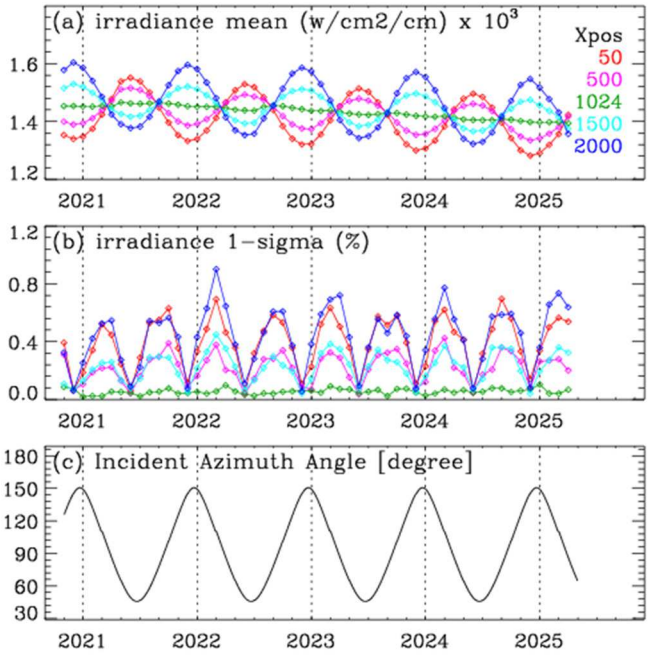

Fig. 2. (a) Monthly mean and (b) 1σ standard deviation of irradiance measurements at 400.2 nm (the center of the spectral pixels) from November 2020 to February 2025, with different colors indicating five selected spatial pixels (50th, 500th, 1024th, 1500th, and 2000th). (c) Daily incident azimuth angle during GEMS irradiance observations. The vertical dashed lines mark each January.

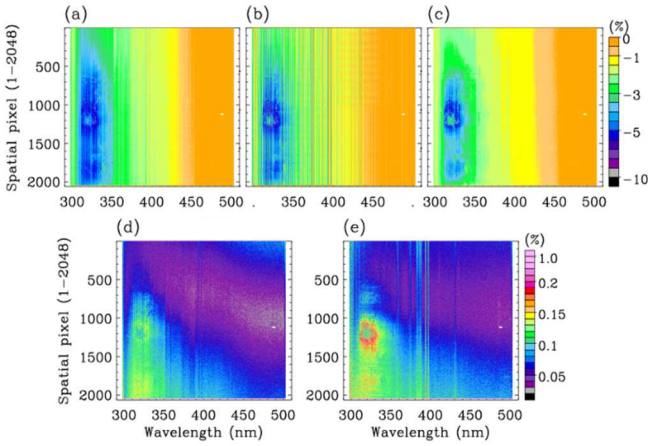

Fig. 3. (a)–(c) Relative changes in the monthly mean irradiance for June between consecutive years from 2021 to 2024, as a function of the full CCD dimension. (d) and (e) Standard deviations of daily irradiance for June 2021 and June 2024. A nonlinear color scale is applied to enhance visualization.

increases to as much as 5%. Overall, the degradation pattern remains consistent from 2021 to 2024, but the intensification of Fraunhofer features between 2022 and 2023 suggests a potential inconsistency in spectral stability. Fig. 3(d) and (e) also compares the standard deviations of irradiance measurements across the CCD frame for June 2021 and 2024, respectively. The daily variability in irradiance is particularly evident in the 310–330-nm range, where the radiometric degradation rate is highest. A comparison between years shows an overall increase in noise by 2024, indicating progressive degradation

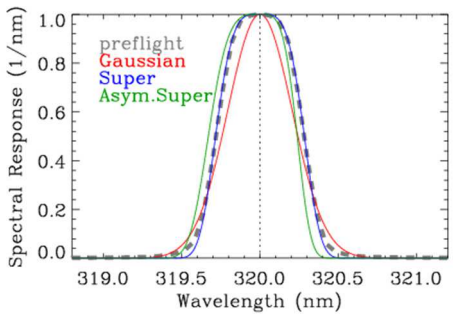

Fig. 4. Preflight ISRF at 320 nm for the center pixel and its derivations from 310 to 330 nm on November 2, 2020, based on three assumed functional forms: Gaussian, super-Gaussian, and asymmetric super-Gaussian.

in instrument stability. In addition, enhanced variability at Fraunhofer lines further suggests growing inconsistencies in spectral stability over time.

B. Evaluation of Derived On-Orbit Slit Functions

On-orbit variations in ISRFs and wavelength shifts have been widely used as key indicators for monitoring the spectral stability of spectrometers, thereby ensuring consistent measurements of the same spectral features over time [2], [3], [26], [29], [30], [31]. The on-orbit slit functions of GEMS, derived using an asymmetric super-Gaussian shape, showed close agreement with the preluanch ISRFs [15]. However, this monitoring was limited to the first year of operation. Furthermore, the wavelength stability has not yet been discussed in the literature.

In practice, correlations among fitting parameters can lead to instability and even divergence in the iterative fitting process. Therefore, it is important to carefully select independent parameters that have a distinct and significant impact on the spectral response.

The initial experiment aims to evaluate the impact and necessity of including asymmetry parameters in the GEMS slit function fitting. According to [26], who introduced super-Gaussian shapes for slit function characterization, we adhere to three key considerations.

1) A two-step fitting process is applied for asymmetric shapes: the first step fits the parameters k and ω, and the second step fits the asymmetric parameters a_k and a_ω.
2) The impact of including each asymmetric term is evaluated by comparing three configurations: Sa (a_ω, a_k = 0), Sa (a_ω = 0, a_k), and Sa (a_ω, a_k).
3) The wavelength shift is incorporated in the first step to mitigate the additional variability arising from correlations with a_k, a_w, differing from [26] where it was treated as a third step.

Fig. 4 illustrates GEMS spectral response functions at 320 nm for the center pixel, comparing on-orbit derivations with preflight measurements. As shown, the preflight ISRF is closely reproduced by the symmetric super-Gaussian fit, which better captures both the peak and wing regions than either the standard Gaussian or the asymmetric super-Gaussian. To support GEMS level 2 data processing, four types of super-Gaussian functions are further evaluated across four spectral ranges used in retrievals: 310–330 nm (O_3 profile, SO_2), 330–360 nm (HCHO), 426–460 nm (NO_2, glyoxal), and 460–490 nm (aerosol height, cloud), as summarized in Table I. Experiment I evaluates the symmetric super-Gaussian, while Experiments II–IV introduce different sets of asymmetric parameters. As shown, the inclusion of a_ω leads to unstable fitting results, causing divergence or out-of-boundary issues (fourth column of Table I). The simultaneous fitting of a_k and a_ω further exacerbates this problem due to their correlation (Experiment II). This configuration results in substantial deviations of +2.35% in the shape factor ($k \pm a_k$) and −13.63% in slit width ($\omega \pm a_\omega$) for the spectral range of the ozone profile (310–330 nm). These deviations are reduced to −0.95% and −3.68%, respectively, when a_k and a_ω are fit separately (Experiments III and IV). On the other hand, the impact of including asymmetry factors on the spectral responses is relatively negligible in the longer UV spectral ranges above 400 nm, where the shape factor and slit width deviate by less than 1%. Nevertheless, the symmetric super-Gaussian remains the preferred choice overall in terms of fitting stability and accuracy. Furthermore, Fig. 5 compares the mean fitting residuals as a function of spatial pixels, confirming that the symmetric shapes provide a better representation of GEMS ISRFs across the full spectral range and all spatial pixels.

C. Spectral Stability: On-Orbit Slit Functions and Wavelength Calibration

Section III-B demonstrated that, among the alternative slit function models, the symmetric super-Gaussian provides the best fit for GEMS's spectral response. Accordingly, this model is adopted to assess the spectral stability of irradiance measurements in terms of the slit widths and wavelength shifts. To characterize their wavelength dependence, spectral fitting is performed at 5-nm intervals. In addition, the sensitivity of the fitting results to window widths of 5, 10, and 20 nm is assessed. Fig. 6 presents the fitting results for November 2021, with vertical bars indicating the temporal variability, bounded by the maximum and minimum values. The FWHMs [see Fig. 6(a)] range from 0.56 to 0.58 nm, exhibiting minor fluctuations without significant wavelength dependence. However, a closer examination reveals features that reflect the sensitivity of the fitting results to spectral structures and uncertainties.

1) *300–370 nm:* Temporal fluctuations are minimal, and the window width has no noticeable effect on the FWHM.
2) *370–450 nm:* A systematic bias in FWHM emerges depending on the fitting window width. This bias may be affected by the presence of different Fraunhofer lines in the solar spectrum, such as the Fe (382 nm), Ca II K (393.4 nm), and Ca II H (396.8 nm), since their inclusion or exclusion can alter the fitting results.
3) *450–500 nm:* When narrower fitting windows are used, the derived FWHM values exhibit greater fluctuations, both in their temporal variability and wavelength dependence. This suggests that spectral fitting is more sensitive to radiometric uncertainties, likely due to the weaker spectral features in the solar spectrum.

Compared to the FWHMs, the wavelength shift shows minimal dependence on the fitting window width and exhibits low temporal variability. However, a distinct wavelength dependence is observed, with the shift gradually varying from +0.05

TABLE I

RATIO BETWEEN SYMMETRIC AND ASYMMETRIC SHAPE PARAMETERS (a_k/k, a_ω/ω), PRESENTED AS THE MEDIAN VALUE OF FITTING RESULTS FROM IRRADIANCE MEASUREMENTS ON NOVEMBER 2, 2020. THE RMS (%) REPRESENTS THE ROOT MEAN SQUARE OF FITTING RESIDUALS BETWEEN MEASURED AND SIMULATED IRRADIANCES. THE NUMBER OF FAILED FITTINGS DUE TO DIVERGENCE (ITERATION > 10) AND OUT-OF-FIT VALUES IS INCLUDED IN THE LAST COLUMNS

Experiment I: S($a_\omega = 0, a_k = 0$)					**Experiment II: S(a_ω, a_k)**				
Spectral range (nm)	k	ω (nm)	RMS (%)	N of failed fittings$^+$	Spectral range (nm)	a_k/k (%)	a_ω/ω (%)	RMS (%)	N of failed fittings
310-330	3.84	0.31	0.344	**3**	300-360	2.35	-13.63	1.062	177
330-360	3.69	0.31	0.589	3	330-360	1.24	-4.82	1.067	184
402-460	3.38	0.32	0.425	0	402-460	0.08	-0.13	0.500	19
460-490	2.90	0.32	0.254	0	460-490	0.98	-0.54	0.256	0
Experiment III: S($a_\omega, a_k = 0$)					**Experiment IV: S($a_\omega = 0, a_k$)**				
Spectral range (nm)	a_k/k (%)	a_ω/ω (%)	RMS (%)	N of failed fittings	Spectral range (nm)	a_k/k (%)	a_ω/ω (%)	RMS (%)	N of failed fittings
310-330	-	-3.68	1.245	108	310-330	-0.95	-	1.350	4
330-360	-	0.03	1.112	94	330-360	0.08	-	1.135	5
402-460	-	0.05	0.507	13	402-460	0.03	-	0.507	0
460-490	-	-0.17	0.257	0	460-490	0.90	-	0.257	0

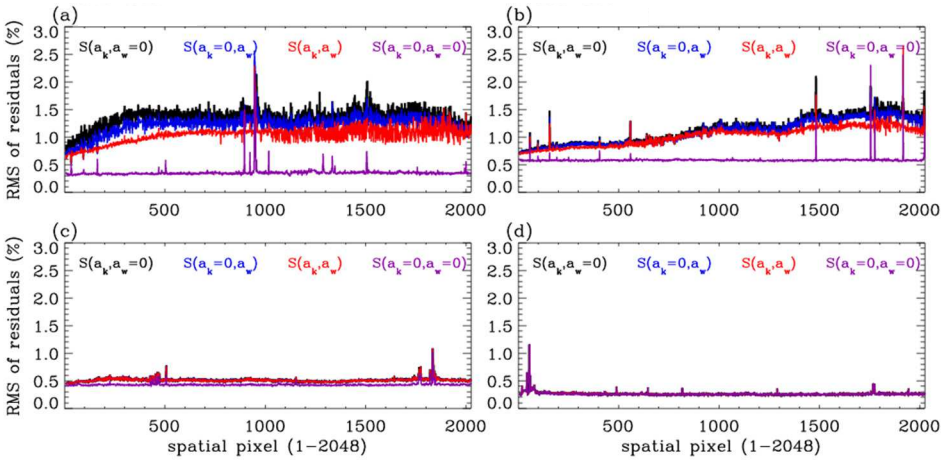

Fig. 5. Impact of applying various super-Gaussian models to derive the GEMS slit functions from (a) 310–330, (b) 330–360, (c) 426–460, and (d) 460–490 nm. The plots show the rms of spectral fit residuals (%) between measured and simulated irradiances as a function of spatial pixels on November 30, 2020.

to −0.05 nm across both 330–395 and 405–470 nm. This smooth transition suggests a stable but systematic wavelength offset rather than random fluctuations. A notable feature is the discontinuity near 400 nm, where a sudden deviation interrupts the otherwise uniform shift pattern. This discontinuity originates from the Level 1C data processing, in which the GEMS data are read out in four quadrants—spatially and spectrally divided at the center—and the wavelength registration is corrected separately for the 300–400- and 400–500-nm ranges, as described in Section II-A.

To provide practical insights into spectral calibration stability, we characterize the spatiotemporal variations of key spectral parameters—slit width, wavelength shift, and fitting reisduals (rms, %)—across the spectral fitting windows used in level 2 retrievals: 310–330 nm (O3, SO2), 330–360 nm (HCHO), 426–460 nm (NO2, CHOCHO), and 460–490 nm (aerosol effective height, cloud), as well as 360–390 and 410–430 nm. Fig. 7 compares the fitting results as a function of spatial pixels on December 15, 2020, and 2024. Overall, the slit width remains stable over time, featuring consistent patterns over the spatial pixels for different fitting windows. However, in the spectral range of 310–330 nm, fluctuations of approximately ±0.05 nm emerge in the center spatial pixels due to degradation. For wavelength shifts, spatial variations are generally minimal, except in the 460–490-nm range, where a smile pattern is evident. As degradation progressed, a "frown-shaped" pattern developed in the fitting windows below 390 nm. In general, the wavelength shift gradually increases toward the center by 0.005 nm between 2021 and 2024. However, in the 310–330-nm range, a sudden increase occurs, with shifts rising abruptly from 0.05 to 0.075 nm in the center pixels (800–1400). In 410–430 and 426–460 nm, a slight but systematic increase in wavelength shift is observed across all spatial pixels. Meanwhile, the 460–490-nm range exhibits enhanced pixel-to-pixel fluctuations. These findings suggest that spectral stability varies by wavelength, with the most pronounced degradation occuring in the shorter UV region (310–330 nm), consistent with radiometric stability

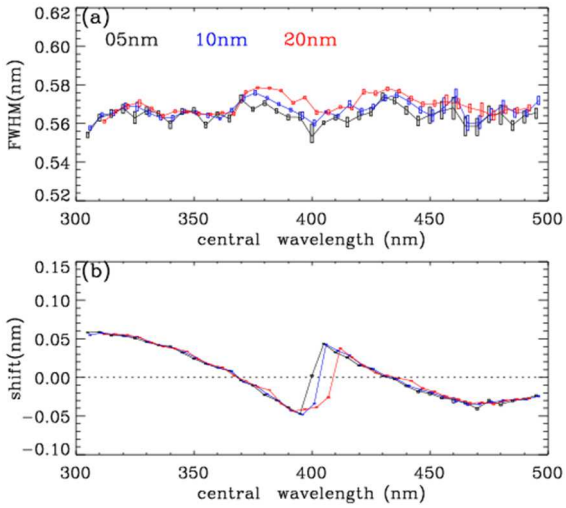

Fig. 6. Wavelength dependence of (a) FWHM and (b) spectral shift between GEMS solar irradiance and the TSIS-1 solar reference, derived from one month of GEMS irradiance data (November 2020). The results are calculated at 5-nm intervals using different fitting window widths (black: 5 nm, blue: 10 nm, and red: 20 nm). The symbols represent the monthly mean values at the center wavelength of the fitting window, and the vertical bars indicate the range between the minimum and maximum values.

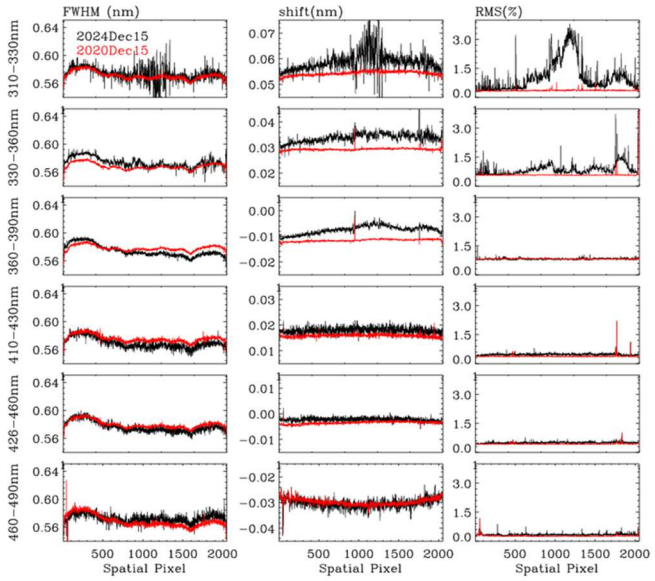

Fig. 7. Slit width, wavelength shift, and fitting accuracy (rms of fitting residuals, %) as a function of spatial pixels on December 15, 2020, and 2024, with different wavelength windows indicated in the *y*-axis titles.

characteristics, as evaluated in Section III-A. The fitting residuals (rms, %) represent the fitting accuracy of GEMS irradiances to the solar reference. In the longer UV range, the radiometric offset is well accounted for in the fitting process, resulting in no significant changes with aging. In contrast, the fitting residuals of 310–330 nm exhibit a faster degradation toward the center pixels. This degradation effect peaks at the 1200th pixel (rms = 4%) and the 1800th pixel (rms = 1.8%) in 2024, whereas, in 2021, the rms remains 0.3% across all cross-track pixels. In the 330–360-nm range, fitting uncertainties

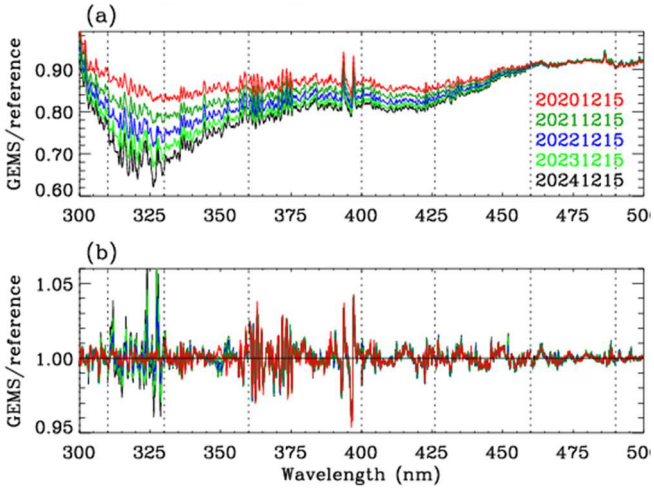

Fig. 8. Yearly variations in irradiance normalized by a reference spectrum at the center spatial pixel (1024th) on December 15 from 2020 to 2024. The reference spectrum is simulated from a high-resolution solar spectrum (a) without and (b) with radiometric adjustment, respectively. The vertical dashed lines indicate the fitting windows used.

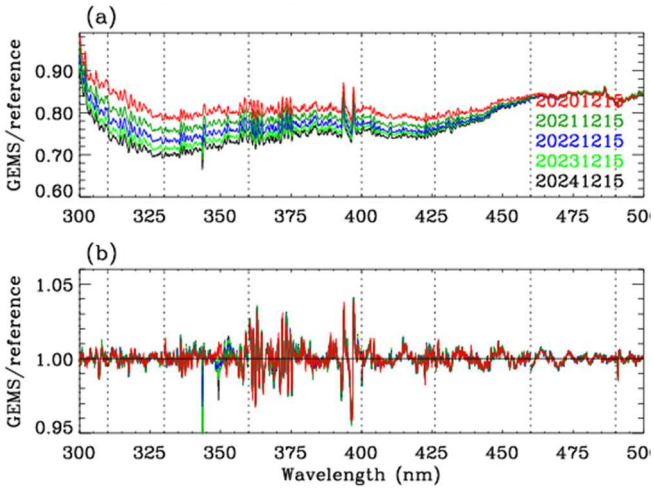

Fig. 9. Yearly variations in irradiance normalized by a reference spectrum at the center spatial pixel (100th) on December 15 from 2020 to 2024. The reference spectrum is simulated from a high-resolution solar spectrum (a) without and (b) with radiometric adjustment, respectively. The vertical dashed lines indicate the fitting windows used.

remain 0.8% in 2021 but increase to 1.8% at the 1800th pixel in 2024.

D. Radiometric Stability

We assess radiometric performance using two diagnostic metrics: 1) the overall radiometric offset and 2) spectral fitting residuals after systematic bias removal, which are used to examine fine-scale structural uncertainties. To quantify the radiometric offset in the GEMS irradiance, the high-resolution TSIS-1 spectrum is convolved with the instrument's slit functions, and wavelength shifts in the measured spectrum are adjusted relative to Fraunhofer lines, as described in (1). As expected, the overall residuals are largely dominated by angle-dependent biases associated with BTDF effects, which hinder the identification of the underlying error sources. To address this, we simulate the reference

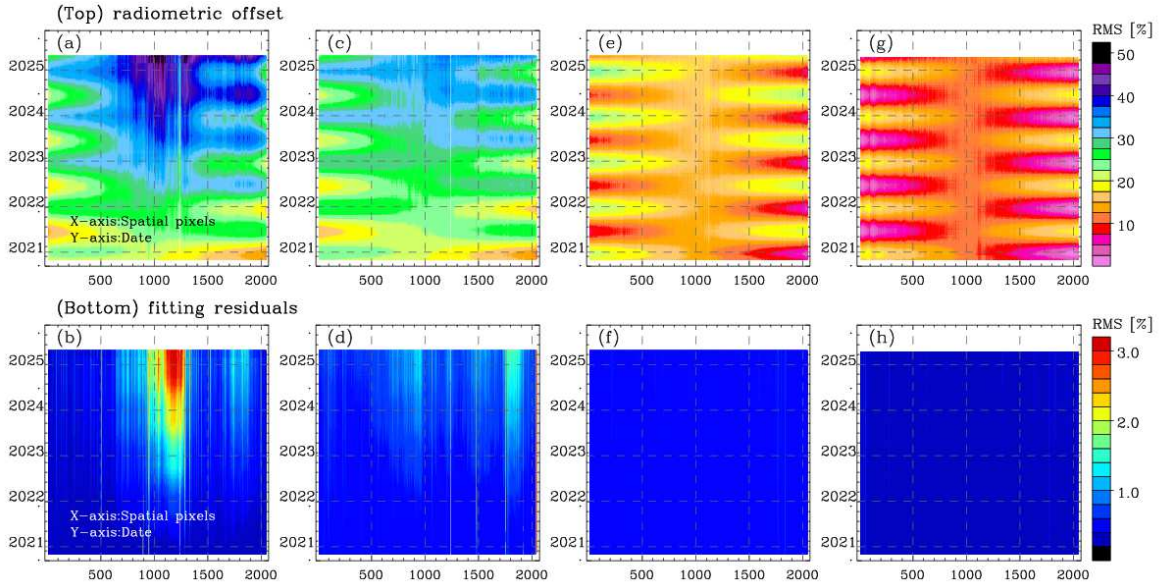

Fig. 10. Spatial and temporal variations in the RMS of radiometric uncertainties (%) over four main spectral ranges. (Top) Radiometric offset is calculated using the spectrally adjusted solar reference. (Bottom) Reference spectrum is adjusted both spectrally and radiometrically to evaluate GEMS irradiances. (a) and (b) 310–330, (c) and (d) 330–360, (e) and (f) 426–460, and (g) and (h) 460–490 nm.

spectrum using (2), which incorporates baseline and scaling adjustments to mitigate the systematic bias. As the reference spectrum is fit both spectrally and radiometrically, the resulting residuals are referred to as spectral fitting residuals.

Figs. 8 and 9 illustrate long-term changes in the radiometric performance on December 15 for five time points between 2020 and 2024 at the center pixel and north edge pixel, respectively. As shown, the systematic offsets are clearly observed over the entire wavelength range, with noticeable temporal variation below 450 nm. At 325 nm, the radiometric offset deepens from 18% in 2020 to 35% in 2024 at the center pixel [see Fig. 8(a)], while a 10% change is observed at the edge pixel over the same period [see Fig. 9(a)]. Beyond 450 nm, the residual offset consistently remains ~10% at the center pixel and ~20% at the edge pixel throughout the years. This stronger degradation at shorter wavelengths, also reported for other satellite instruments including OMI, OMPS, and TROPOMI [3], [32], [33], is attributed to solar diffuser exposure to UV radiation and energetic particles. At the center pixel, in particular, the irradiance in 310–330 nm exhibits increasingly pronounced and newly emerging spectral structures over time. While the irradiance-to-reference ratio initially shows minimal variation across neighboring wavelengths, by 2024, fluctuations exceed 10% within the ozone fitting window (310–330 nm) [see Fig. 8(a)]. The spectral residuals between GEMS and the radiometrically adjusted solar reference [see Fig. 8(b)] also reveal temporal peaks, exceeding ±5%, compared to less than ±1% in 2020. In 360–400 nm, fine-scale structured residuals are consistently observed over time at both center and edge pixels. These features arise from discrepancies in Fraunhofer structures (380–400 nm) between the GEMS irradiance and the reference spectrum, as well as uncertainties in the spectral adjustment of the reference spectrum due to wavelength-dependent shifts in GEMS, which vary within ±0.05 nm [see Fig. 6].

We further evaluate the spatiotemporal changes in radiometric performance [see Fig. 10]. The overall discrepancy between irradiance and reference is primarily driven by seasonally dependent radiometric offsets peaking at the summer solstice and at the winter solstice. In the center pixels, striping patterns have been consistently observed since the beginning of observations. As degradation progresses, these stripes extend further toward the southern pixels in 310–330 nm. A significant discrepancy, reaching up to 40%, appears in 2023 near the 1100th–1300th pixels, which further expands to the 700th pixel by late 2024. In addition, the striping patterns spread into the 330–360-nm range in 2022. While seasonal and spatial offsets are generally mitigated by baseline and scaling terms in the fitting process, residual striping errors and abrupt degradation features remain uncorrected [see Fig. 10(b) and (d)].

IV. Conclusion and Discussion

This study presents a comprehensive evaluation of the long-term radiometric accuracy and spectral stability of GEMS based on 4.5 years of solar irradiance observations. Our analysis reveals a progressive decrease in radiometric values, with an annual decline of 5% at shorter wavelengths and 0.2% at longer wavelengths. In addition, short-term noise increases over the mission duration. The midsection of the CCD, particularly near the short UV pixels, exhibits the most pronounced long-term changes and short-term variability. Spectral stability in GEMS operational products is assessed using three diagnostic metrics across all retrieval fitting windows: spectral response repeatability, wavelength shift, and spectral fit rms. As the first step in this assessment, we revisit the methodology for determining ISRFs in orbit. A previous study [15] recommended the use of an asymmetric super-Gaussian model to characterize GEMS ISRFs. However, our analysis reveals that incorporating asymmetric parameters results in unstable fitting, leading to a twofold to threefold increase in

fitting residuals for 310–330 and 330–360 nm. Therefore, the symmetric super-Gaussian model is adopted to evaluate slit variables and determine the wavelength shift relative to the high-resolution solar reference. The derived slit widths exhibit minimal wavelength dependence, whereas the wavelength shift of irradiance relative to the reference spectrum varies linearly between 330–395 and 415–470 nm, within a range of ± 0.05 nm. Notably, finer and deeper fluctuating structures in the 360–460-nm range—observed in the spectral residuals between irradiance and the solar reference—are associated with wavelength-dependent shifts, emphasizing the need for wavelength-dependent corrections. As degradation progresses from 2020 to 2024, wavelength shifts increase toward the center of the spatial pixels for wavelengths below 400 nm. Particularly, the 310–330-nm range exhibits severe degradation in the central spatial pixels, where wavelength shifts reach up to 0.07 nm, and FWHM fluctuates significantly between 0.54 and 0.60 nm. In addition, fitting uncertainties rise sharply, increasing from 0.4% to 4%.

Compared to the solar reference, GEMS irradiances exhibit a maximum deviation of 18% near 325 nm and a minimum deviation of 10% above 450 nm. By 2024, the radiometric discrepancy increases to 35% at 325 nm. The spectrally broadened offset is largely corrected by the baseline and scaling adjustments, allowing the spectral fitting process to remove most seasonal and spatial variations, particularly in the longer UV ranges. However, residual degradation features distort intrinsic solar absorption structures and introduce artificial fine-scale features. The resulting striping artifacts, initially observed in the center pixels between 310 and 330 nm, gradually extend toward the southern pixels and progressively affect a broader spectral range (300–360 nm) over the course of the mission.

The findings of this study have important implications for the reliability of GEMS data and its applications in atmospheric research. The identified degradation patterns and calibration biases directly affect the accuracy of GEMS data products, particularly for ozone profiles that rely on spectral fitting in 310–330 nm. Addressing these issues through improved calibration strategies, including refined spectral corrections and radiometric degradation adjustments, is essential for enhancing the reliability of GEMS-derived ozone measurements and ensuring their consistency with other satellite-based observations.

REFERENCES

[1] M. Dobber et al., "Validation of ozone monitoring instrument level 1b data products," *J. Geophys. Res., Atmos.*, vol. 113, no. D15, pp. 1–12, Apr. 2008, doi: 10.1029/2007jd008665.

[2] Q. Kleipool et al., "Ozone monitoring instrument (OMI) collection 4: Establishing a 17-year-long series of detrended level-1b data," *Atmos. Meas. Techn.*, vol. 15, no. 11, pp. 3527–3553, Jun. 2022, doi: 10.5194/amt-15-3527-2022.

[3] V. M. E. Schenkeveld et al., "In-flight performance of the ozone monitoring instrument," *Atmos. Meas. Techn.*, vol. 10, no. 5, pp. 1957–1986, Jun. 2017, doi: 10.5194/amt-10-1957-2017.

[4] R. Munro et al., "The GOME-2 instrument on the metop series of satellites: Instrument design, calibration, and level 1 data processing—An overview," *Atmos. Meas. Techn.*, vol. 9, no. 3, pp. 1279–1301, Mar. 2016, doi: 10.5194/amt-9-1279-2016.

[5] I. Kutiev et al., "Solar activity impact on the Earth's upper atmosphere," *J. Space Weather Space Climate*, vol. 3, p. A06, Feb. 2013, doi: 10.1051/swsc/2013028.

[6] B. Mendoza, "Total solar irradiance and climate," *Adv. Space Res.*, vol. 35, no. 5, pp. 882–890, May 2005, doi: 10.1016/j.asr.2004.10.011.

[7] J. Bak et al., "An improved OMI ozone profile research product version 2.0 with collection 4 L1b data and algorithm updates," *Atmos. Meas. Techn.*, vol. 17, no. 7, pp. 1891–1911, Apr. 2024, doi: 10.5194/amt-17-1891-2024.

[8] J. Kim et al., "New era of air quality monitoring from space: Geostationary environment monitoring spectrometer (GEMS)," *Bull. Amer. Meteorological Soc.*, vol. 101, no. 1, pp. E1–E22, Jan. 2020, doi: 10.1175/bams-d-18-0013.1.

[9] K. Baek, J. H. Kim, J. Bak, D. P. Haffner, M. Kang, and H. Hong, "Evaluation of total ozone measurements from geostationary environmental monitoring spectrometer (GEMS)," *Atmos. Meas. Techn.*, vol. 16, no. 22, pp. 5461–5478, Nov. 2023, doi: 10.5194/amt-16-5461-2023.

[10] Y. Cho et al., "First atmospheric aerosol-monitoring results from the geostationary environment monitoring spectrometer (GEMS) over Asia," *Atmos. Meas. Techn.*, vol. 17, no. 14, pp. 4369–4390, Jul. 2024, doi: 10.5194/amt-17-4369-2024.

[11] E. S. Ha et al., "First evaluation of the GEMS glyoxal products against TROPOMI and ground-based measurements," *Atmos. Meas. Techn.*, vol. 17, no. 21, pp. 6369–6384, Nov. 2024, doi: 10.5194/amt-17-6369-2024.

[12] S. S. Park et al., "Retrieval algorithm for aerosol effective height from the geostationary environment monitoring spectrometer (GEMS)," *Atmos. Meas. Techn.*, vol. 18, no. 10, pp. 1–40, May 2025, doi: 10.5194/amt-18-2241-2025.

[13] P. Zoogman et al., "Tropospheric emissions: Monitoring of pollution (TEMPO)," *J. Quant. Spectrosc. Radiat. Transf.*, vol. 186, pp. 17–39, Jan. 2017, doi: 10.1016/j.jqsrt.2016.05.008.

[14] G. B. Courrèges-Lacoste et al., "The Copernicus sentinel 4 mission: A geostationary imaging UVN spectrometer for air quality monitoring," *Proc. SPIE*, vol. 10423, pp. 62–70, Mar. 2017.

[15] M. Kang et al., "Characteristics of the spectral response function of geostationary environment monitoring spectrometer analyzed by ground and in-orbit measurements," *IEEE Trans. Geosci. Remote Sens.*, vol. 60, 2022, Art. no. 5509916, doi: 10.1109/TGRS.2021.3091677.

[16] M. Kang et al., "On-orbit correction of bi-directional transmittance distribution function (BTDF) of geostationary environment monitoring spectrometer (GEMS)," *IEEE Trans. Geosci. Remote Sens.*, vol. 62, 2024, Art. no. 5540315, doi: 10.1109/TGRS.2024.3510337.

[17] J. Kim, H. Chong, Y. Cho, S. Lee, and Y. Ki, "Geostationary environment monitoring spectrometer (GEMS) level-1C user guide," Environmental Satellite Center, National Institute of Environmental Research, Ministry of Environment, Incheon, South Korea, Tech. Rep. 1.0, 2020.

[18] J. J. Butler, G. T. Georgiev, and C. C. Cooksey, "Comparison of bidirectional transmittance distribution function (BTDF) measurements on fused silica and sintered polytetrafluoroethylene diffusers," *Metrologia*, vol. 56, no. 6, Dec. 2019, Art. no. 065008, doi: 10.1088/1681-7575/ab4523.

[19] J. Fu et al., "Development of primary reference facilities and measurement comparison of standard artifacts for the bidirectional transmittance distribution function," *Rev. Scientific Instrum.*, vol. 94, no. 8, Aug. 2023, doi: 10.1063/5.0151803.

[20] O. M. Coddington et al., "The TSIS-1 hybrid solar reference spectrum," *Geophys. Res. Lett.*, vol. 48, no. 12, pp. 1–10, Jun. 2021, doi: 10.1029/2020gl091709.

[21] K. Lee et al., "Pioneering air quality monitoring over east and Southeast Asia with the geostationary environment monitoring spectrometer (GEMS)," *Korean J. Remote Sens.*, vol. 40, nos. 5–2, pp. 741–752, Oct. 2024, doi: 10.7780/kjrs.2024.40.5.2.5.

[22] K. Chance and R. L. Kurucz, "An improved high-resolution solar reference spectrum for Earth's atmosphere measurements in the ultraviolet, visible, and near infrared," *J. Quant. Spectrosc. Radiat. Transf.*, vol. 111, no. 9, pp. 1289–1295, Jun. 2010, doi: 10.1016/j.jqsrt.2010.01.036.

[23] J. Brion, A. Chakir, D. Daumont, J. Malicet, and C. Parisse, "High-resolution laboratory absorption cross section of O3. Temperature effect," *Chem. Phys. Lett.*, vol. 213, nos. 5–6, pp. 610–612, Oct. 1993, doi: 10.1016/0009-2614(93)89169-i.

[24] P. Lindström and P.-Å. Wedin, "Methods and software for nonlinear least squares problems," Univ. Umeå, Umeå, Sweden, Tech. Rep. UMINF-133.87, 1988.

[25] J. Bak et al., "Impact of using a new high-resolution solar reference spectrum on OMI ozone profile retrievals," *Remote Sens.*, vol. 14, no. 1, p. 37, Dec. 2021, doi: 10.3390/rs14010037.

[26] S. Beirle, J. Lampel, C. Lerot, H. Sihler, and T. Wagner, "Parameterizing the instrumental spectral response function and its changes by a super-Gaussian and its derivatives," *Atmos. Meas. Techn.*, vol. 10, no. 2, pp. 581–598, Feb. 2017, doi: 10.5194/amt-10-581-2017.
[27] T. N. Woods, J. W. Harder, G. Kopp, and M. Snow, "Solar-cycle variability results from the solar radiation and climate experiment (SORCE) mission," *Sol. Phys.*, vol. 297, no. 4, p. 43, Apr. 2022, doi: 10.1007/s11207-022-01980-z.
[28] O. Coddington et al., "Solar irradiance variability: Comparisons of models and measurements," *Earth Space Sci.*, vol. 6, no. 12, pp. 2525–2555, Dec. 2019, doi: 10.1029/2019ea000693.
[29] K. Sun et al., "Deriving the slit functions from OMI solar observations and its implications for ozone-profile retrieval," *Atmos. Meas. Techn.*, vol. 10, no. 10, pp. 3677–3695, Oct. 2017, doi: 10.5194/amt-10-3677-2017.
[30] J. Bak, X. Liu, K. Sun, K. Chance, and J.-H. Kim, "Linearization of the effect of slit function changes for improving ozone monitoring instrument ozone profile retrievals," *Atmos. Meas. Techn.*, vol. 12, no. 7, pp. 3777–3788, Jul. 2019, doi: 10.5194/amt-12-3777-2019.
[31] M. Kang, M.-H. Ahn, X. Liu, U. Jeong, and J. Kim, "Spectral calibration algorithm for the geostationary environment monitoring spectrometer (GEMS)," *Remote Sens.*, vol. 12, no. 17, p. 2846, Sep. 2020, doi: 10.3390/rs12172846.
[32] Z. Zhang, J. Niu, L. E. Flynn, E. Beach, and T. Beck, "An approach to track instrument calibration and produce consistent products with the version-8 total column ozone algorithm (V8TOZ)," *Atmos. Meas. Techn.*, vol. 16, no. 11, pp. 2919–2941, Jun. 2023, doi: 10.5194/amt-16-2919-2023.
[33] A. Ludewig et al., "In-flight calibration results of the TROPOMI payload on board the Sentinel-5 precursor satellite," *Atmos. Meas. Techn.*, vol. 13, no. 7, pp. 3561–3580, Jul. 2020, doi: 10.5194/amt-13-3561-2020.

Juseon Bak received the M.S. and Ph.D. degrees in atmospheric science from Pusan National University, Busan, South Korea, in 2011 and 2015, respectively.

From 2017 to 2020, she was a Post-Doctoral Research Associate at the Harvard-Smithsonian Center for Astrophysics, Cambridge, MA, USA. She is currently a Research Scientist with the Institute of Environmental Studies, Pusan National University. She has contributed to the development of operational ozone profile retrieval algorithms for GEMS, TEMPO, and OMI PROFOZ Collection four product. She has also participated in several international projects, including ACCLIP, Asian-AQ 2024, and TOAR-II (2020–2024). Her research interests include analysis of ultraviolet–visible–near-infrared spectra for detecting atmospheric composition related to air quality and climate.

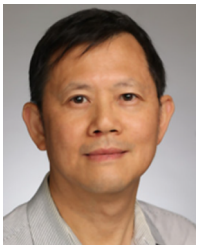

Kai Yang received the Ph.D. degree in physics from Kansas State University, Manhattan, KS, USA.

He has extensive experience in remote sensing of atmospheric trace gases, aerosols, and clouds, with expertise in algorithm development, data product creation, and instrument calibration. He has contributed to numerous NASA and NOAA missions and has served as the Principal Investigator (PI) for multiple awards, including NASA's NO2 and SO2 environmental data records from SNPP OMPS, NASA's O3 and volcanic SO2 products from DSCOVR/EPIC, and NOAA's advanced NO2 product from OMPS on the JPSS satellite series. Currently, he is the PI for the enterprise NO2 algorithm for NOAA's Geostationary Extended Observations (GeoXO) Atmospheric Composition sensor (ACX), set to launch in the next decade.

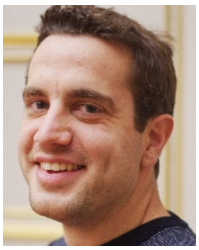

Arno Keppens received the master's degree in physics from UGent, Ghent, Belgium, in 2006, and the Ph.D. degree in engineering from KU Leuven, Leuven, Belgium, in 2010.

He was a Post-Doctoral Guest Researcher at the National Institute of Standards and Technology (NIST), Gaithersburg, MD, USA. He is a Senior Scientist in remote sensing at the Royal Belgian Institute for Space Aeronomy (BIRA-IASB), Brussels, Belgium, where he is mostly responsible for the independent quality assessment of multiple satellite datasets.

Dr. Keppens is a member of the Belgian and European Physical Societies.

Mijeong Kim received the B.S. and M.S. degrees in atmospheric science from Pusan National University, Busan, South Korea, in 2015 and 2017, respectively. She is currently pursuing the Ph.D. degree in atmospheric science.

Since 2020, she has been a Researcher at the Environmental Satellite Center, Atmospheric Environmental Research Department, National Institute of Environmental Research (NIER), Incheon, South Korea. She is currently engaged in the development of artificial intelligence-based retrieval algorithms for the Geostationary Environmental Monitoring Spectrometer (GEMS). Her research interests include the operation and enhancement of the Level-1B processing algorithm for the GEMS.

Xiong Liu received the B.S. degree in environmental chemistry from Nankai University, Tianjin, China, in 1995, the M.S. degree in environmental chemistry from the Research Center for Eco-Environmental Sciences, Chinese Academy of Sciences, Beijing, China, in 1998, and the M.S. degree in computer science and the Ph.D. degree in atmospheric science from The University of Alabama in Huntsville, Huntsville, AL, USA, in 2002.

He is currently a Senior Physicist with the Center for Astrophysics—Harvard & Smithsonian Center, Cambridge, MA, USA. He is the Principal Investigator of the Tropospheric Emissions: Monitoring of Pollution (TEMPO) Project and leads the Atmospheric Measurements Group at Harvard & Smithsonian Center. His research interests include the remote sensing of atmospheric trace gases, aerosols, and clouds, satellite mission development, and instrument calibration.

Dr. Liu is a member of American Geophysical Union and American Meteorological Society. He received TEMPO Group Achievement Awards from NASA in 2013, 2020, and 2024, the William T. Pecora Award to OMI International Science Team in 2018, the AMS Special Award to OMI International Science Team in 2020, and the Advances in Atmospheric Science Outstanding Editor Awards in 2023 and 2024.

Jae-Hwan Kim received the B.S. degree from the Department of Physics, Pusan National University, Busan, South Korea, and the Ph.D. degree from the Department of Meteorology, University of Maryland, College Park, MD, USA.

He is currently a Professor with the Department of Atmospheric Science, Pusan National University, and has dedicated his career to the study of remote sensing for atmospheric ozone and clouds. He leads a research team for satellite ozone retrieval of GEMS, the first environmental monitoring satellite from geostationary Earth orbit (GEO).

Jhoon Kim (Member, IEEE) received the B.S. degree in atmospheric sciences from Seoul National University, Seoul, South Korea, and the Ph.D. degree in atmospheric and space sciences from the University of Michigan, Ann Arbor, MI, USA.

He was the Principal Researcher at Korea Aerospace Research Institute, Daejeon, South Korea. He is a Yonsei Lee Youn Jae Fellow Professor of atmospheric science at Yonsei University, Seoul, South Korea, and has dedicated his career to the study of remote sensing for aerosols and trace gases, including air pollutants and greenhouse gases. He is the Principal Investigator (PI) of GEMS, the first satellite instrument for air quality monitoring from geostationary Earth orbit (GEO) at unprecedented spatiotemporal resolution. He is also a member of the Committee on Earth Observation Satellites (CEOS) AC-VC, where he has contributed to the establishment of a coordinated GEO constellation for global air quality observation. He served as the Director for the establishment of the Particulate Matter Research Institute, Samsung Advanced Institute of Technology (SAIT), Suwon, South Korea. He has authored over 250 articles.

Dr. Kim is a fellow of the Korean Academy of Science and Technology (KAST). He served as a Guest Editor for *Atmospheric Measurement Techniques*.

Myoung-Hwan Ahn (Member, IEEE) received the B.S. degree in atmospheric sciences from Seoul National University, Seoul, South Korea, in 1987, and the Ph.D. degree in meteorology from the University of Maryland, College Park, MD, USA, in 1997.

His doctoral thesis is on the development of an algorithm to retrieve SO_2 from the TOMS instrument onboard the Nimbus-7 satellite. Before joining the current affiliation, Ewha Womans University in Seoul, Korea, as a Professor, in 2012, he had worked for the Korea Meteorological Administration (KMA) as a Senior Researcher. During his career at KMA, he led a group of scientists to develop the level 2 data processing system of the meteorological imager onboard a multipurpose geostationary satellite, which is the first Korean meteorological satellite. After successful commissioning of the first satellite and related data processing system, he laid out the follow-on GK-2 satellite program. His research interests are centered around the GK-2 program, including instrument characterization, retrieval theory, and information content for the atmospheric profiles that are closely related to the retrieval algorithm for the AMI and GEMS of the GK-2 satellites, as well as cloud detection using ground-based passive instruments such as the infrared thermometer, and utilization of remote sensing data for the numerical weather prediction model.

Heesung Chong received the B.S. degree in chemical and biomolecular engineering and the Ph.D. degree in atmospheric sciences from Yonsei University, Seoul, South Korea, in 2015 and 2021, respectively.

He is currently a Physicist with the Center for Astrophysics—Harvard & Smithsonian, Cambridge, MA, USA. He is currently a Science Team Member of the Tropospheric Emissions: Monitoring of Pollution (TEMPO) mission. His primary research interests include the retrieval of trace gas concentrations in the Earth's atmosphere from remote sensing measurements and the characterization and calibration of satellite instruments.

Sungjae Hong received the B.S. and M.S. degrees from Pusan National University (PNU), Busan, South Korea, where he is currently pursuing the Ph.D. degree in atmospheric science.

He has worked as a Research Assistant at PNU and is currently involved in the GEMS project, where he focuses on ozone profile validation. His major field of study is satellite meteorology and the numerical weather prediction system. His research interests include satellite-based atmospheric analysis, air quality monitoring, and numerical weather prediction.

Kyunghwa Lee received the M.S. and Ph.D. degrees in environmental science from Gwangju Institute of Science and Technology (GIST), Gwangju, South Korea, in 2013 and 2018, respectively.

She is currently a Researcher with the Environmental Satellite Center, Atmospheric Environmental Research Department, National Institute of Environmental Research (NIER), Incheon, South Korea. Her research interests include applications of satellite data to improve understanding of the atmospheric environment by analyzing the optical and chemical properties of air pollutants, filling gaps in satellite observations, and conducting data assimilation using chemical transport models combined with multiplatform observations from satellites and ground-based in situ measurements.

Mina Kang received the B.S. degree in electronic engineering and the Ph.D. degree in atmospheric science and engineering from Ewha Womans University, Seoul, South Korea, in 2010 and 2021, respectively.

From 2021 to 2024, she was a Post-Doctoral Researcher at Ewha Womans University. She is currently a Research Scientist with the Research Foundation of the City University of New York and the National Oceanic and Atmospheric Administration Cooperative Science Center for Earth System Sciences and Remote Sensing Technologies (NOAA-CESSRST), New York, NY, USA. Her research interests include validating level 2 products from the Tropospheric Emissions: Monitoring of Pollution (TEMPO) mission using ground-based observations and atmospheric composition forecast models, calibration and validation of satellite and airborne instruments, and contributions to the Global Space-based Inter-Calibration System (GSICS) for ultraviolet and visible sensors.

Won-Jin Lee (Member, IEEE) received the M.S. and Ph.D. degrees in geoinformatics from the University of Seoul, Seoul, South Korea, in 2010 and 2015, respectively.

He is currently a Senior Researcher with the Environmental Satellite Center, National Institute of Environmental Research, Incheon, South Korea. Recently, he has been focusing on the development of the Geostationary Environment Monitoring Spectrometer (GEMS) algorithm and application. Also, the InSAR method to assess and predict risks is associated with geophysical hazards. His research interests include the estimation and correction of InSAR processing and performance improvements of surface deformation measurement using multitemporal InSAR (MTInSAR) techniques.

Hyunkee Hong received the M.S. degree in atmospheric science from Yonsei University, Seoul, South Korea, and the Ph.D. degree in engineering from Pukyong National University, Busan, South Korea.

He was responsible for the initial development of the NO_2 algorithm for the Geostationary Environment Monitoring Spectrometer (GEMS). After joining the National Institute of Environmental Research (NIER), Incheon, South Korea, he has been in charge of the development and validation of GMES products, as well as the establishment of an Asian ground-based remote sensing network for GEMS validation.